AIAA JOURNAL
Vol. 44, No. 3, March 2006

Space-Time Least-Squares Spectral Elements for Convection-Dominated Unsteady Flows

B. De Maerschalck*
Von Kármán Institute for Fluid Dynamics, 1640 Sint-Genesius-Rode, Belgium
M. I. Gerritsma†
Delft University of Technology, 2629 HS Delft, The Netherlands
and
M. M. J. Proot‡
Shell Global Solutions International B.V., 1031 CM Amsterdam, The Netherlands

Legendre polynomials are employed in a space-time least-squares spectral element formulation applied to linear and nonlinear hyperbolic scalar equations. No stabilization techniques are required to render a stable, high-order-accurate scheme. In parts of the domain where the underlying exact solution is smooth, the scheme exhibits exponential convergence with polynomial enrichment, whereas in parts of the domain where the underlying exact solution contains discontinuities the solution displays a Gibbs-like behavior. Numerical results will be given in which the capabilities of the space-time formulation to capture discontinuities will be demonstrated.

Introduction

THE least-squares spectral element method (LSQ-SEM) was developed by Proot[1] and Proot and Gerritsma.[2,3] The method combines the least-squares formulation as described in Jiang and coworkers[4–9] and Bochev and coworkers[10–17] with a spectral element approximation as described in Canuto et al.[18] and Karniadakis and Sherwin.[19] Recently, a space-time formulation of the LSQ-SEM has been applied to linear and nonlinear hyperbolic scalar equations using Legendre polynomials[§] and Chebyshev polynomials.[20] According to Laney[21] the linear advection equation and the nonlinear Burgers equation are the building blocks in computational gasdynamics, where the linear advection equation models entropy waves exhibiting contact discontinuities, and the nonlinear Burgers equation models the nonlinear interaction of waves with different wave numbers, which can lead to the development of shocks and expansion fans.

Spectral methods perform best when the underlying exact solution is sufficiently smooth, and therefore spectral methods have mainly been used in elliptic/parabolic problems. The use of spectral methods in hyperbolic problems, which allow for discontinuous solutions, "traditionally has been viewed as problematic,"[22] and therefore comparatively little work has been done.

Least-Squares Formulation

Bona fide least-squares formulations form an interesting alternative to Galerkin and Petrov–Galerkin weak formulations for the discretization of partial differential equations.[5,6,16] The least-squares method converts well-posed partial differential equations into symmetric positive-definite algebraic equations, irrespective of the type of the underlying partial differential equation. Furthermore, the least-squares approach circumvents compatibility requirements in mixed/constrained formulations, which implies that no inf-sup condition between the approximating velocity space and the approximating pressure space needs to be imposed. These features allow a unified approach of a variety of flows encountered in aerospace engineering, such as compressible vs incompressible and avoids the directional dependence of the numerical scheme in subsonic, transonic, and supersonic flows.

The least-squares approach is based on the minimization of a norm-equivalent functional. Consider a system of first-order linear partial differential equations and boundary conditions:

$$\mathbb{L}\boldsymbol{u} = \boldsymbol{f} \qquad \text{in} \qquad \Omega \tag{1}$$

$$\mathbb{B}\boldsymbol{u} = \boldsymbol{g} \qquad \text{on} \qquad \Gamma \tag{2}$$

Assume that the system is well posed so that two Hilbert scales $X_q(\Omega)$ and $Y_q(\Omega) \times Y_q(\Gamma)$ exist, such that $(\mathbb{L}, \mathbb{B})$ has a complete set of homeomorphisms, that is, the mapping $\boldsymbol{u} \mapsto (\mathbb{L}\boldsymbol{u}, \mathbb{B}\boldsymbol{u})$ is a homeomorphism $X_q(\Omega) \mapsto Y_q(\Omega) \times Y_q(\Gamma)$ for all q, with q a scale parameter, for example, with $q = 0$ one obtains the L^2 space and $q = 1$ refers to the H^1 space. The least-squares formulation seeks for a minimum of the residuals of Eqs. (1) and (2) in a certain norm. The norm-equivalent functional then becomes

$$\mathcal{J}(\boldsymbol{u}) = \tfrac{1}{2}\left[\|\mathbb{L}\boldsymbol{u} - \boldsymbol{f}\|^2_{Y_q(\Omega)} + \|\mathbb{B}\boldsymbol{u} - \boldsymbol{g}\|^2_{Y_q(\Gamma)}\right] \tag{3}$$

Notice that minimizing $\mathcal{J}(\boldsymbol{u})$ and solving Eqs. (1) and (2) in the least-squares sense are equivalent. Minimizing the functional $\mathcal{J}$ for $\boldsymbol{u}$ means the following: find $\boldsymbol{u}$, so that

$$\lim_{\varepsilon \to 0} \frac{\mathrm{d}}{\mathrm{d}\varepsilon} \mathcal{J}(\boldsymbol{u} + \varepsilon \boldsymbol{v}) = 0, \qquad \forall \boldsymbol{v} \in X_q \tag{4}$$

Equivalently, one can write the necessary condition as follows: Find $\boldsymbol{u} \in X_q$ such that

$$\mathcal{B}(\boldsymbol{u}, \boldsymbol{v}) = \mathcal{F}(\boldsymbol{v}), \qquad \forall \boldsymbol{v} \in X_q \tag{5}$$

where $\mathcal{B}(\boldsymbol{u}, \boldsymbol{v}) = (\mathbb{L}\boldsymbol{u}, \mathbb{L}\boldsymbol{v})_{Y_q(\Omega)} + (\mathbb{B}\boldsymbol{u}, \mathbb{B}\boldsymbol{v})_{Y_q(\Gamma)}$ is a symmetric, continuous bilinear form and $\mathcal{F}(\boldsymbol{v}) = (\boldsymbol{f}, \mathbb{L}\boldsymbol{v})_{Y_q(\Omega)} + (\boldsymbol{g}, \mathbb{B}\boldsymbol{v})_{Y_q(\Gamma)}$ is a continuous linear functional.

The inclusion of the boundary residual in Eq. (3) allows for the use of minimization spaces $X_q(\Omega)$, which are not constrained to

Received 14 May 2003; presented as Paper 2003-3684 at the AIAA 16th Computational Fluid Dynamics Conference, Orlando, FL, 23–26 June 2003; accepted for publication 1 September 2005.

*Member, Doctoral Program, Waterloosesteenweg 72; demaersc@vki.ac.be.
†Member, Scientific Staff, Aerospace Engineering, Kluyverweg 1; M.I.Gerritsma@lr.tudelft.nl.
‡Team Member, Multiphase Flow, Badhuisweg 3; michael.proot@shell.com.
§Data available online at http://www.aero.lr.tudelft.nl/~bart [cited 12 March 2003].

satisfy the boundary condition (2); that is, the boundary conditions are enforced weakly through the variational principle. This is advantageous whenever the boundary condition is difficult to satisfy computationally and represents an additional beneficial feature of least-squares based methods. If, on the other hand, Eq. (2) can be easily imposed, one can consider Eq. (3) with the boundary term omitted. Then the functions belonging to the space $X_q(\Omega)$ should be required to satisfy the boundary condition, that is, Eq. (2) is enforced strongly or directly on candidate minimizers.

We now have a framework for developing a least-squares finite element method for Eqs. (1) and (2). Given the boundary-value problem, one can proceed as follows:

1) Choose a functional setting, that is, two Hilbert scales $X_q(\Omega)$ and $Y_q(\Omega) \times Y_q(\Gamma)$.

2) Choose between variational (weak) or direct (strong) enforcement of the boundary conditions and set up the relevant least-squares functional, that is, Eq. (3) with or without the boundary residual term, respectively.

3) Fix the scale parameter q, for example, choose $q = 0$.

4) Choose a finite dimensional subspace $X_q^h \subset X_q$ parameterized by $h \to 0$, where h can refer to a characteristic mesh width, polynomial degree, or a combination of both.

5) Restrict Eq. (5) to X_q^h.

This process leads to a discrete variational problem, namely, seek $\boldsymbol{u}^h \in X_0^h$ such that

$$\mathcal{B}(\boldsymbol{u}^h, \boldsymbol{v}^h) = \mathcal{F}(\boldsymbol{v}^h), \qquad \forall \boldsymbol{v}^h \in X_0^h \tag{6}$$

with

$$\mathcal{B}(\boldsymbol{u}^h, \boldsymbol{v}^h) = \int_{\Omega_e} \mathbb{L}\boldsymbol{u}^h \, \mathbb{L}\boldsymbol{v}^h \, \mathrm{d}\Omega$$

$$\mathcal{F}(\boldsymbol{v}^h) = \int_{\Omega_e} \boldsymbol{f} \, \mathbb{L}\boldsymbol{v}^h \, \mathrm{d}\Omega$$

Spectral Elements

In the preceding section we briefly discussed the general idea of the least-squares approach. Now we turn to the finite dimensional subspace $X_0^h(\Omega)$, mentioned earlier. In spectral element methods, the computational domain is subdivided into small nonoverlapping subdomains Ω_i called spectral elements. To achieve high-order accuracy both in space and in time, space-time elements have been introduced. This means that the "fourth" dimension, time, is considered as an additional spatial dimension. Therefore, for a one-dimensional time-dependent problem, two-dimensional spectral elements are required. These spectral elements are then mapped onto a standard element $[-1, 1] \times [-1, 1]$. Within this standard element the approximate solution is expanded in space-time basis functions:

$$u^h(x,t) = u^{P,Q}(x,t) = \sum_{i=1}^{P+1} \sum_{j=1}^{Q+1} u_{i,j}^h H_{i,j}(x,t) \tag{7}$$

with

$$H_{i,j}(x,t) = h_i(x)\, h_j(t) \tag{8}$$

where the basis functions $h_i(x)$ are Lagrangian interpolants through the Gauss–Lobatto–Legendre (GLL) points.[18,23] The basis functions are explicitly given by

$$h_i(x) = \frac{(x-1)\,(x+1)\,L'_P(x)}{P\,(P+1)\,L_P(x_i)\,(x-x_i)} \tag{9}$$

with $1 \le i \le P+1$. $L_P(x)$ is the Legendre polynomial of degree P, and x_i are the $P+1$ GLL points, that is, the $P-1$ zeros of the first derivative of the Legendre polynomial $L'_P(x)$ supplemented with the boundary nodes ($x_1 = -1$ and $x_{P+1} = 1$). Figure 1 shows four of the 49 space-time shape functions for a spectral element of order $P = Q = 6$. The Lagrange polynomial $h_i(x)$ is the unique polynomial of degree P, which has a unit value at x_i and is zero at x_j $(j \neq i)$, $h_i(x_j) = \delta_{ij}$; therefore, holds $u^h(x_i, t_j) = u_{i,j}^h$.

The derivative of the Lagrangian basis functions (9), evaluated at the Gauss–Lobatto–Legendre points, are given by

$$\left.\frac{\mathrm{d}h_j}{\mathrm{d}x}\right|_{x_i} = \begin{cases} \dfrac{L_P(x_i)}{L_P(x_j)} \dfrac{1}{(x_i - x_j)}, & i \neq j,\ 1 \le i, j \le P+1 \\ 0, & 1 < i = j < P+1 \\ -\dfrac{1}{4}P(P+1), & i = j = 1 \\ \dfrac{1}{4}P(P+1), & i = j = P+1 \end{cases} \tag{10}$$

Integrals are evaluated numerically using the Gauss–Lobatto integration rule:

$$\int_{-1}^{1} f(x)\,\mathrm{d}x \approx \sum_{i=1}^{P+1} w_i\, f(x_i) \tag{11}$$

where x_i represent the $P+1$ distinct GLL points in the interval $[-1\ 1]$, and w_i are the GLL weights with

$$w_i = \int_{-1}^{1} h_i(x)\,\mathrm{d}x = \frac{2}{P(P+1)[L_P(x_i)]^2} \tag{12}$$

Application to Hyperbolic Problems

Numerical schemes to solve hyperbolic problems usually take the direction of the wave velocity into account. Because the least-squares approach leads to a symmetric formulation, this requirement is no longer necessary. The main question therefore is, How well does the least-squares spectral element formulation perform in problems that have a strong directional dependence? To answer this question, LSQ-SEM will be applied to linear and nonlinear hyperbolic problems.

Results for the Linear Advection Equation

The first test case consists of a linear advection problem given by

$$\frac{\partial u}{\partial t} + a\frac{\partial u}{\partial x} = 0, \qquad 0 \le x \le L, \qquad t \ge 0 \tag{13}$$

with

$$u(0,x) = u_0(x), \qquad u(t,0) = u(t,L) \tag{14}$$

The exact solution of this problem is given by

$$u(t,x) = u_0(x - at) \tag{15}$$

So the initial profile is convected with a constant speed through the computational domain. The physical relevance of this model problem is that it models entropy waves in gasdynamics.

The following test cases will be considered:

1) The linear advection of a smooth cosine function on a periodic domain with initial condition is

$$u_0(x) = \tfrac{1}{2}[1 - \cos(2\pi x)], \qquad 0 \le x \le L = 1 \tag{16}$$

Because the solution is infinitely smooth, we do not expect spurious wiggles. Furthermore, one can expect exponential convergence with polynomial enrichment (increasing the polynomial degree). To assess the stability, calculations for various Courant–Friedrichs–Lewy (CFL) numbers will be presented with

$$\mathrm{CFL} = a(P/Q)(\Delta t/\Delta x) \tag{17}$$

where Δt is the size of the spectral element in the time direction and Δx is the size of the spectral element in the spatial dimension.

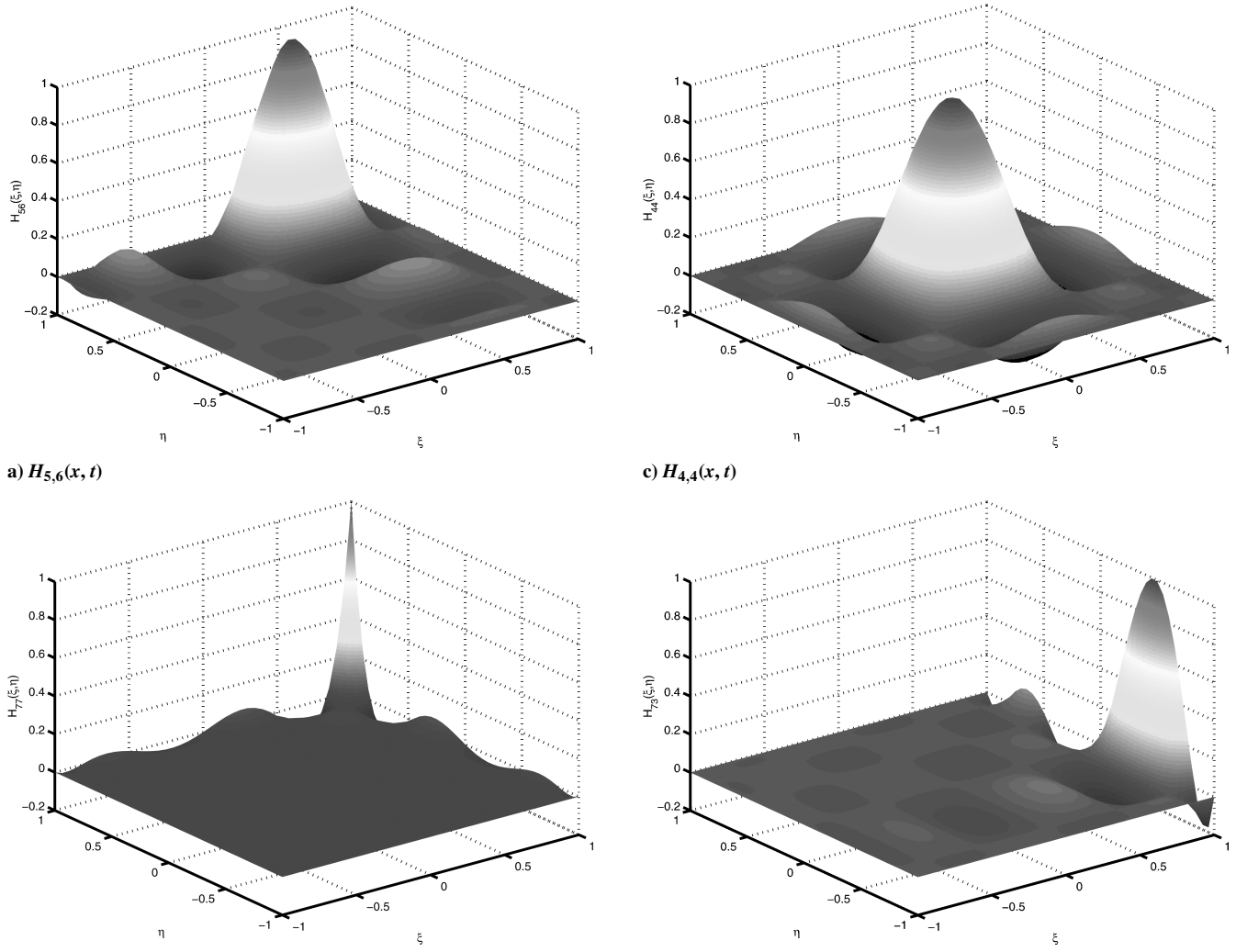

Fig. 1 Four of the 49 space-time shape functions $H_{i,j}(x,t) = h_i(x)h_j(t)$ of order $P = Q = 6$.

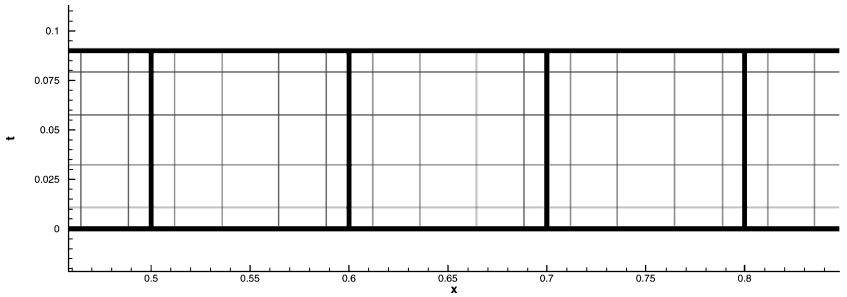

Fig. 2 Spectral element space-time strip with number of cells per unit length $N_c/UL = 10$ and order $P = Q = 5$.

2) The linear advection of a square wave on a periodic domain with initial condition is

$$u_0(x) = \begin{cases} 1 & \text{for} \quad 0.25 \le x \le 0.75 \\ 0 & \text{elsewhere} \end{cases} \tag{18}$$

In this case the length of the domain is chosen $L = 4$. This solution is discontinuous, and we do not expect exponential convergence with polynomial enrichment. Furthermore, we expect wiggles around the discontinuities similar to the wiggles we observe around a discontinuity in approximation theory.

A detail of the space-time spectral element grid that is used each time step is shown in Fig. 2. This is an equispaced rectangular spectral element mesh consisting of 10 cells per unit length in the x direction, denoted by N_c/UL, and one cell in the temporal direction. The polynomial interpolation order for each cell is in both directions the same with $P = Q = 5$, where P refers to the polynomial degree in space and Q denotes the polynomial degree in time.

Figures 3 and 4 show the results of the LSQ-SEM for the advection of the initial cosine function and initial square wave at a fixed time level ($T = 10$) for different CFL numbers. These plots demonstrate that there is no need to add dissipative terms to stabilize the scheme. This makes the scheme low diffusive, which is particularly important for the approximation of Navier–Stokes equations and for long time integration. When we apply the initial square wave to the linear advection problem, spurious Gibbs phenomena can be observed (Fig. 4), as was expected. From the plots one observes that right in front of and right behind the discontinuities the approximate solution is polluted by spurious oscillations. However, when plotting the

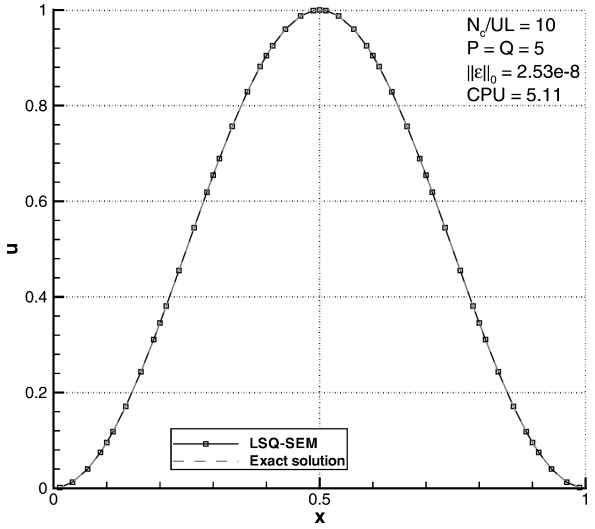

a) CFL = 0.1

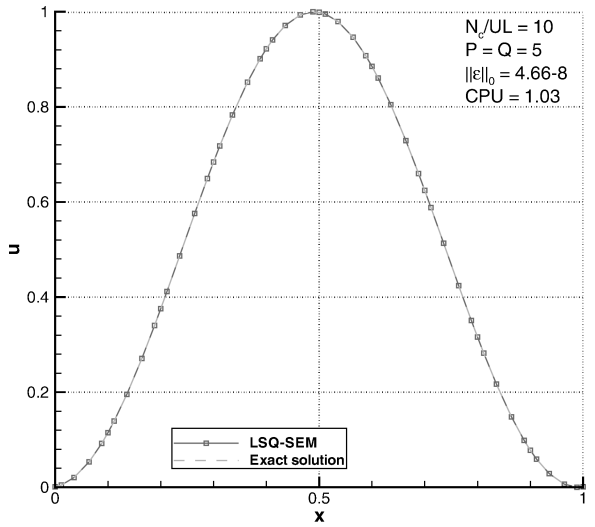

b) CFL = 0.9

Fig. 3 Linear advection of an initial cosine function. LSQ-SEM solution at a fixed time level $T = 10$, for different CFL numbers (grid: $N_e/UL = 10$, $P = Q = 5$).

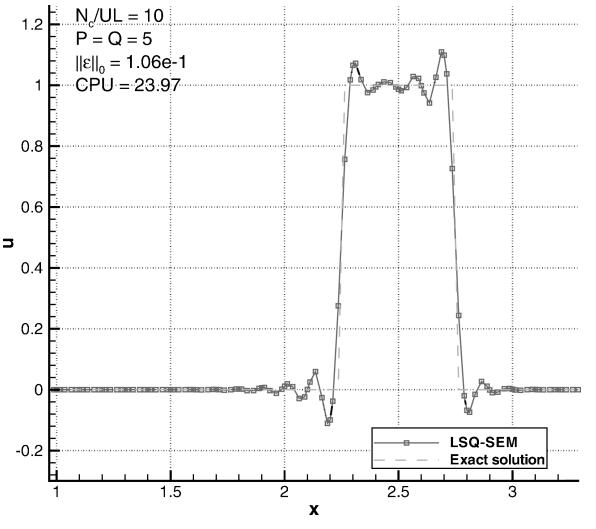

a) CFL = 0.1

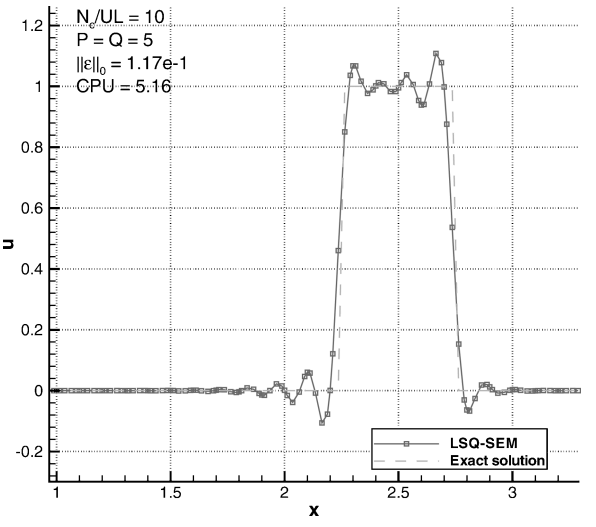

b) CFL = 0.9

Fig. 4 Linear advection of an initial square wave. LSQ-SEM solution at a fixed time level $T = 10$, for different CFL numbers (grid: $N_e/UL = 10$, $P = Q = 5$).

minimum and maximum value of the solution in time (Fig. 5), one observes that the oscillations do not tend to grow in time. Both plots in Fig. 5 again demonstrate the low diffusion error. The amplitude of the cosine remains constant for long time integration. Numerical results show that the Gibbs phenomenon does not pollute the whole domain over time. It is restricted to the direct neighborhood of the discontinuities. No smearing of the discontinuities occurs. This can be noticed in Fig. 6, where the solution is plotted as a contour plot in space-time domain. The white lines indicate the position of the discontinuities with their spurious oscillations. These lines are parallel to each other and do not have the intension to diverge in time. Note however that the main part of the space-time solution domain remains unpolluted in contrast to the space-time Galerkin spectral element formulation, which turns out to be unstable.[§]

From the results for the initial square wave, it is obvious that the least-squares spectral element method is nonmonotone. The spurious oscillations pollute the solution near discontinuities. Even for very fine meshes with high interpolation order, some peaks will show up (for instance, see Fig. 7). Laney describes this phenomenon as follows: "The problem areas due to the Gibbs phenomenon are like those of the ghetto—while you can make the ghetto as small as you like, things are still just as bad for the people left in the ghetto."[21]

Important to notice until now is that the approach is unconditionally stable without the need for artificial diffusion. Because the spurious oscillations are only located close to the discontinuities, there is the possibility of retrieving the location of the discontinuity and of reconstructing a monotonous approximation from the least-squares solution as will be shown later.

Grid-Convergence Study

When applying spectral elements, two types of convergence can be studied. One can increase the number of cells while keeping the polynomial degree of the elements constant (h convergence). It can be proven that when the exact solution $u \in H^s(\Omega)$ the error in the L^2 norm in case of h refinement is given by[1]

$$\|\epsilon\|_0 \leq C\, h^l\, |u|_l \qquad \text{with} \qquad l = \min(P+1, s) \tag{19}$$

where P is the polynomial degree of the spectral elements and h represents a grid parameter, for example, the average length of the cells in the x direction (Δx). The seminorm $|u|_l$ and C are constant for a given problem. In case of a polynomial enrichment, that is, increasing the polynomial degree in all cells while keeping the number of elements constant, exponential convergence is expected for smooth solutions. The error is calculated at the final time level T in the L^2 norm:

$$\|\epsilon\|_0 = \left\{ \int_0^L \left[u^h(x,T) - u_{ex}(x,T) \right]^2 \mathrm{d}x \right\}^{\frac{1}{2}} \tag{20}$$

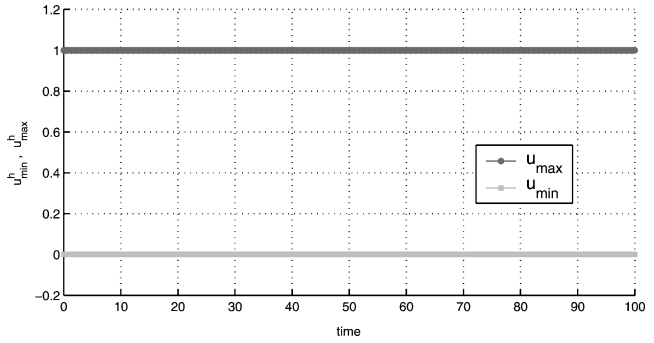

a) Initial cosine

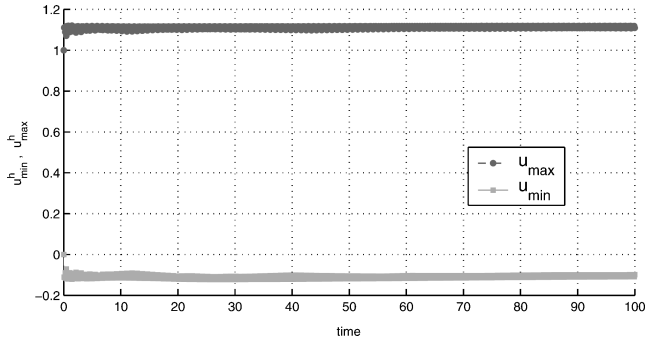

b) Initial square wave

Fig. 5 The $u_{\min}$ and $u_{\max}$ in time for LSQ-FEM applied to the linear advection equation with initial cosine function and initial square wave (grid: $N_e/UL = 10$, $P = Q = 5$, CFL = 0.9).

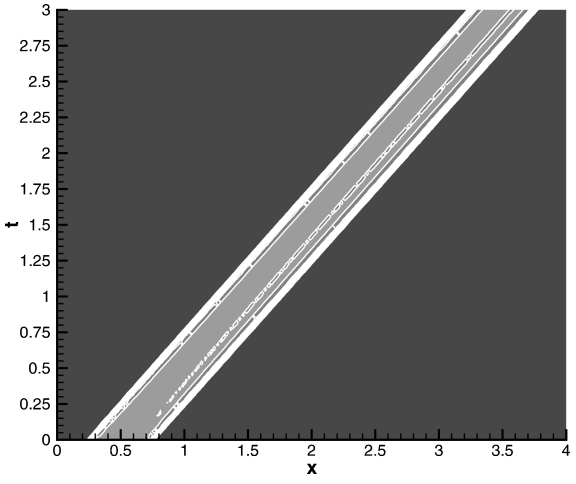

Fig. 6 Space-time contour plot, linear advection of a square wave, CFL = 0.9, $N_e/UL = 10$, $P = Q = 5$.

For the initial cosine function the exact solution is infinitely smooth; therefore, $s = \infty$. The exact solution of the initial square wave contains discontinuities.

It can be proven that $s < 0.5$. For the convergence we expect algebraic convergence both for h- as for p-type refinement, with for the h type a convergence rate of 0.5. Figures 8 and 9 show the results of both convergence types for the smooth (cosine) and nonsmooth (square wave) test cases. Both figures are plotted on a double logarithmic scale. Note the different scales used for the figures. These figures illustrate that indeed the convergence rate is exponential for smooth solutions when p refinement is applied and algebraic in all other cases. When discontinuities appear in the solution, because of the spurious Gibbs phenomenon, the convergence is very slow. However it is noted that in case of polynomial enrichment the convergence rate is still slightly faster than h refinement.

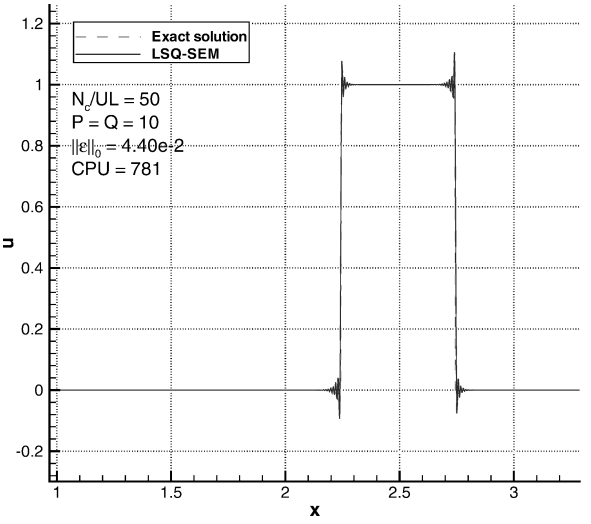

Fig. 7 Linear advection of an initial square wave. LSQ-SEM solution at a fixed time level $T = 10$ (grid: $N_e/UL = 50$, $P = Q = 10$, CFL = 0.9).

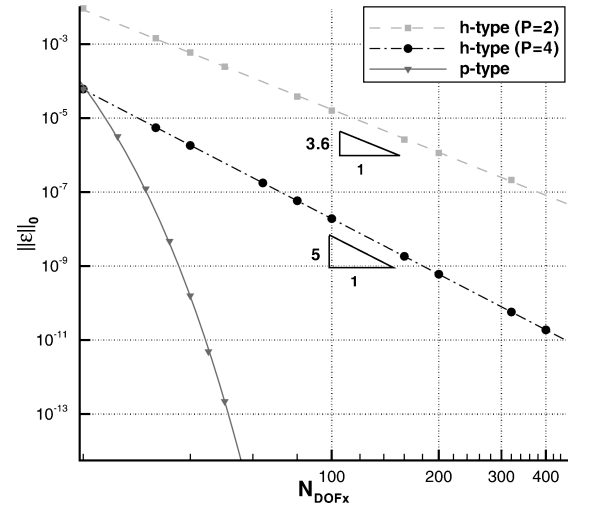

Fig. 8 The *h/p* convergence for the linear advection of the smooth cosine function.

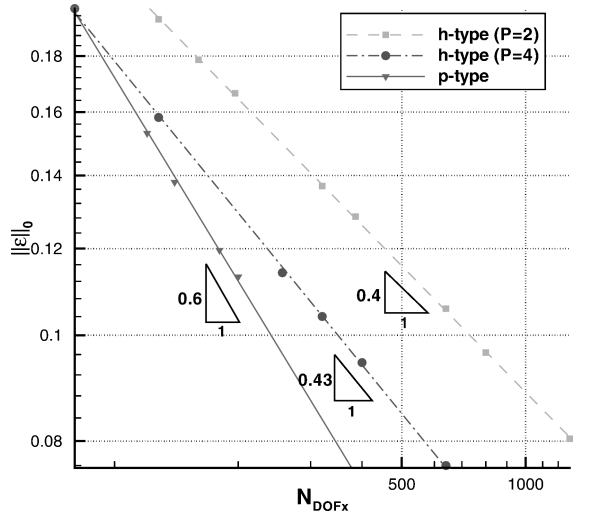

Fig. 9 The *h/p* convergence for the linear advection of the discontinuous square wave.

Results for the Nonlinear Hyperbolic Scalar Equations

The least-squares spectral element method will be applied to the one-dimensional inviscid Burgers equation

$$\frac{\partial u}{\partial t} + \frac{\partial u^2}{\partial x} = 0 \qquad \text{with} \qquad 0 \le x \le L,\ t \ge 0 \tag{21}$$

with initial condition a single cosine hill

$$u_0(x) = \begin{cases} \frac{1}{2}[1 - \cos(\pi x)] & \text{for} \quad 0 \le x \le 2 \\ 0 & \text{elsewhere} \end{cases} \tag{22}$$

Because this equation is nonlinear, linearization of the quadratic term will be required. Two types of linearization have been used: Newton linearization and Picard iteration.

When u^{k-1} and u^k are the solutions of Eq. (21) for two consecutive iteration steps and $\delta u = u^k - u^{k-1}$ is the difference between these two, then one can neglect the higher-order terms of δu and linearize Eq. (21) by

$$\frac{\partial u^k}{\partial t} + 2\left(u^{k-1}\frac{\partial u^k}{\partial x} + u^k \frac{\partial u^{k-1}}{\partial x} - u^{k-1}\frac{\partial u^{k-1}}{\partial x} \right) = 0 \tag{23}$$

To find the discrete solution u^k of Eq. (23) in the least-squares spectral element sense means the following: find u^k, which minimizes the following functional:

$$\mathcal{J}(u^k) = \frac{1}{2}\left\| \frac{\partial u^k}{\partial t} + 2\left(u^{k-1}\frac{\partial u^k}{\partial x} + u^k \frac{\partial u^{k-1}}{\partial x} - u^{k-1}\frac{\partial u^{k-1}}{\partial x} \right) \right\|^2_{L^2} \tag{24}$$

This expression is called the nonconservative Newton LSQ-SEM formulation. The nonconservative Picard linearized formulation only takes the first two terms of Eq. (23) into account; therefore,

$$\mathcal{J}(u^k) = \frac{1}{2}\left\| \frac{\partial u^k}{\partial t} + 2u^{k-1}\frac{\partial u^k}{\partial x} \right\|^2_{L^2} \tag{25}$$

For both iteration types minimizing the functional $\mathcal{J}(u^k)$ in a least-squares finite element sense will lead to positive-definite symmetric system of equations of the form

$$A\boldsymbol{u}^k = \boldsymbol{f} \tag{26}$$

with $\boldsymbol{u}^k$ the solution vector containing the unknown coefficients. The stiffness matrix A and the force vector $\boldsymbol{f}$ are dependent on the previous iteration step. (For Picard only A will be dependent on u^{k-1}.) Therefore Eq. (26) has to be solved various times at each time level.

Figure 10 shows the results for the one-dimensional Burgers equations when the LSQ-SEM is applied using both the nonconservative Newton and Picard formulation. Again the error is calculated in the L^2 norm, and Δx_s is the measured distance between the exact position of the shock discontinuity ($x_s = 3.20978$) and the predicted position of the discontinuity in the LSQ-SEM solution.

At first sight only a slight difference between the two solutions can be noticed. However, when the polynomial degree is increased the Newton formulation seems to have some problems to converge. The shock position is not predicted correctly anymore with increasing polynomial degree. When Picard is used instead, the numerical prediction of the discontinuity does converge to the exact shock position as can be observed in Table 1. It is a remarkable fact that the Newton linearization, when it converges, converges to a different solution than the Picard iteration. This phenomenon is probably because in the presence of large gradients very large entries appear in the stiffness matrix, which makes the system very stiff, in contrast to the Picard iteration in which only the value from a previous iteration appears in the system matrix.

Figure 11 shows a space-time contour plot of the the LSQ-SEM solution for the Burgers equation when the nonconservative Picard formulation is applied. This figure, together with Fig. 6, shows the ability to capture discontinuities that are not aligned to the grid. The white band around the singularity is a result of the local Gibbs phenomenon. Note that because no dissipative terms have been added to the weak solution to stabilize the method, no smearing of the shocks occurs.

Determination of the Location of Discontinuities

The results for the linear and the nonlinear hyperbolic scalar equations just presented demonstrate that the least-squares spectral element method is high-order accurate in the smooth parts of the solution, but exhibit Gibbs-like oscillations near discontinuities in

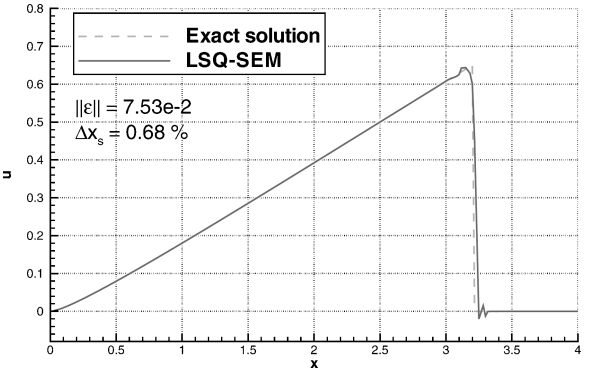

a) Newton

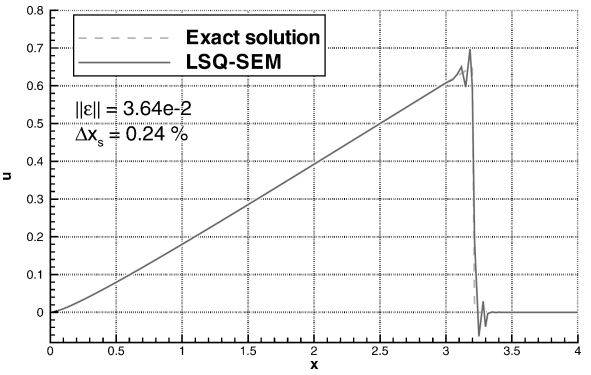

b) Picard

Fig. 10 LSQ-SEM solution of the Burgers equation at time level $T = 2$ ($N_c/UL = 10$, $P = Q = 4$, CFL = 1).

Table 1 Results for the Burgers equation with initial cosine hill for different interpolation degrees ($T = 2$, CFL = 1, $N_c/UL = 10$)

Element order	Newton				Picard			
	$\|\epsilon\|_0$	Δx_s, [%]	N_{tot}	CPU	$\|\epsilon\|_0$	Δx_s, [%]	N_{tot}	CPU
4	$7.53e{-2}$	0.68	620	258	$3.64e{-2}$	0.24	619	234
5	$5.35e{-2}$	1.85	794	531	$5.21e{-2}$	0.24	694	414
6	$2.21e{-1}$	3.41	717	773	$2.94e{-2}$	0.03	785	768
8	No convergence				$1.02e{-2}$	0.01	1254	3737

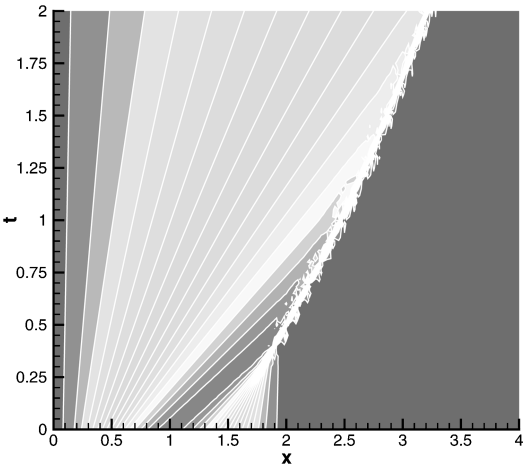

Fig. 11 Space-time contour plot, LSQ-SEM applied to one-dimensional Burgers equation, CFL = 0.9, $N_c/UL = 10$, $P = Q = 5$.

the solution or in its derivatives. Despite the fact that the method converges in the L^2 norm, the error in the minimax norm is $\mathcal{O}(1)$. Recently it has been proven rigorously that the oscillatory behavior around discontinuities is not just noise, but contains sufficient information to reconstruct an exponentially convergent approximation everywhere in the computational domain, provided that the location of the discontinuity is known, that is, the Gibbs phenomenon can be overcome completely.[22,24]

To determine from the oscillatory numerical solution the location of the discontinuity, the enhanced edge detection method developed by Gelb and Tadmor[25] is used. The idea is to expand the numerical solution in a filtered Fourier series

$$\tilde{S}_N^{\sigma}[u^h](x) = \sum_{k=-N}^{N} \tilde{u}_k^h \sigma\left(\frac{k}{N}\right) e^{ikx} \tag{27}$$

which converges faster than the unfiltered Fourier representation ($\sigma = 1$) (Refs. 24 and 25). The factor σ is called the concentration factor. With the use of the particular choice $\sigma = \sigma^r(\xi) = -\pi r \xi^r$, the filtered Fourier representation can be written as

$$\tilde{\mathcal{I}}_N^{\sigma^{2p+1}}[u^h](x) = (-1)^p \frac{\pi(2p+1)}{N^{2p+1}} \frac{\mathrm{d}^{2p+1}}{\mathrm{d}x^{2p+1}} \mathcal{I}_N(u^h)(x) \tag{28}$$

For the particular choice $p = 0$, one obtains

$$S_N[u^h](x) = \frac{\pi}{N} \frac{\mathrm{d}u^h}{\mathrm{d}x} \tag{29}$$

It is proven[25] that S_N converges pointwise to

$$\lim_{N\to\infty} S_N[u^h](x) = u^h(x+\epsilon) - u^h(x-\epsilon), \qquad \epsilon \to 0 \tag{30}$$

So in regions where the solution is continuous, this expression tends to converge to zero, and near discontinuities this expression will yield a finite nonzero value. The location of a discontinuity is then determined from the value $x = x_s$ for which S_N has a sharp peak.

For finite values of N, the expression S_N will be very oscillatory with a more pronounced maximum near the discontinuity. By amplification of the scales, the location of the discontinuity can be filtered out of the spurious oscillations in S_N for finite values of N. Therefore define

$$T_N(x) = N^{q/2}(S_N[u^h](x))^q \to \begin{cases} N^{q/2}[[u^h](x)]^q & \text{if} \quad x = x_s \\ O(N^{-q/2}) & \text{elsewhere} \end{cases} \tag{31}$$

where x_s denotes the position of the discontinuity. The enhanced edge detection method now sets

$$S_N^e[u^h](x) = \begin{cases} S_N[u^h](x) & \text{if} \quad |T_N(x)| > J_{\text{crit}} \\ 0 & \text{if} \quad |T_N(x)| < J_{\text{crit}} \end{cases} \tag{32}$$

Here J_{crit} is an $\mathcal{O}(1)$ threshold parameter, which signifies the critical (minimal) amplitude necessary for jumps to be detected. One has to bear in mind, however, that the polynomial degrees used to solve the differential equation are considered high in comparison to standard finite element methods, but are rather low in comparison to the polynomial degrees used by Gelb and Tadmor. As it turns out, S_N^e gives a good indication of the location of the discontinuity, but its value does not predict the amplitude of the discontinuity correctly. However, a good indicator of the shock position is all we need in this work. Results of the concentration method and enhancement are shown in Fig. 12. The result of the enhanced concentration method is demonstrated in Fig. 13 for the numerical solution of Fig. 10b. Once the discontinuities have been detected, it is possible to reconstruct the solution in the piecewise smooth subdomains defined by the position of the edges and the boundary conditions. Figure 14 shows the result of the postprocessing piecewise reconstruction method applied to the solution of Fig. 10b.

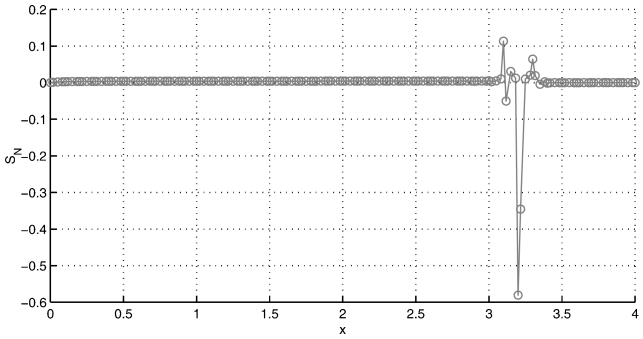

a) $S_N(x)$

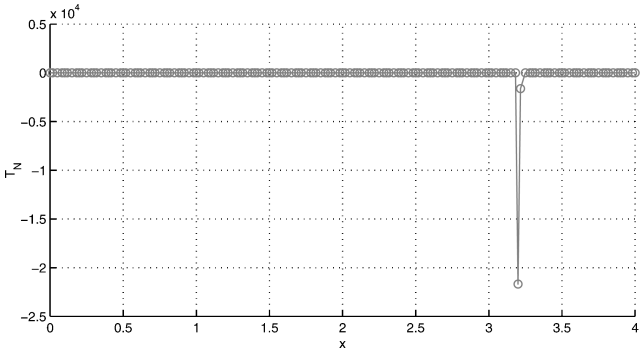

b) $T_N(x)$, with $q = 5$

Fig. 12 Enhanced concentration method applied to the numerical solution of Fig. 10b.

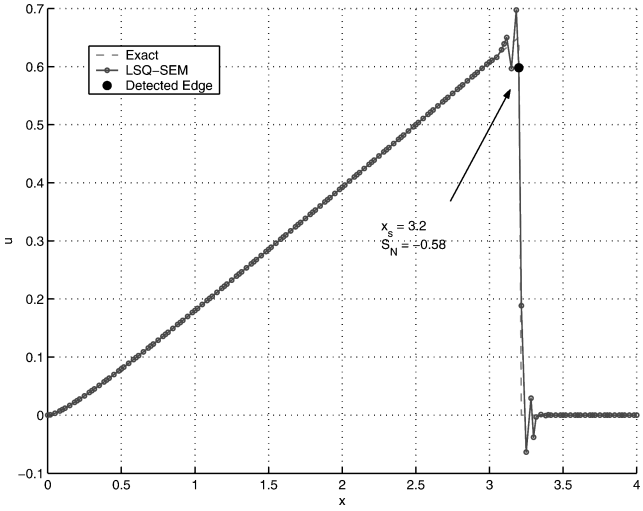

Fig. 13 Result of the edge detection method. The pointed node indicates the detected position of the shock.

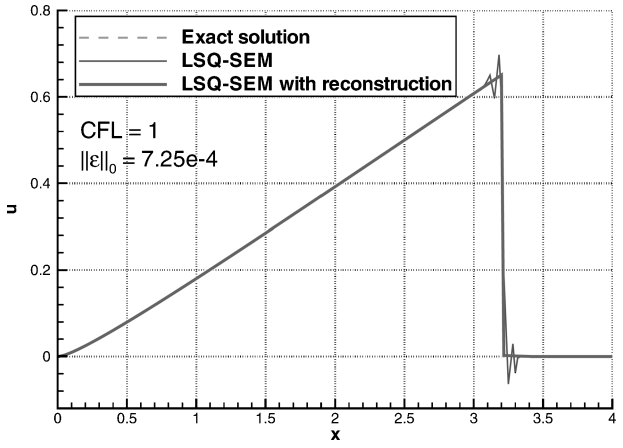

Fig. 14 Piecewise reconstruction method applied to the LSQ-SEM solution of Fig. 10b.

Conclusions

In this paper the space-time least-squares spectral element formulation using Lagrange polynomials has been discussed. The method turns out to be unconditionally stable without the necessity of adding dissipative terms. This make the scheme low diffusive, which is particularly important for long time integration and for the approximation of Navier–Stokes equations. The numerical results also show that the scheme has low dissipative error.

Near discontinuities the numerical solution displays a Gibbs-like behavior, however in elements that do not contain a discontinuity the approximation is unaffected by the presence of oscillations elsewhere in the numerical solution. This remarkable behavior is quite contrary to the behavior observed in the space-time Galerkin spectral element method, where ultimately the whole numerical solution is affected by the presence of discontinuities in case no dissipative terms have been added to the weak formulation.[§] A grid-convergence study shows that in case of polynomial enrichment the LSQ-SEM solution converges exponentially when the underlying exact solution is smooth. In all other cases the convergence is algebraic and depends on the smoothness of the exact solution. Because of the Gibbs-like behavior, the numerical solution converges to the exact solution in the L^2 norm, but not in the L^∞ norm. However, in contrast to conventional schemes for hyperbolic equations, increasing the polynomial degree in the presence of singularities leads to more accurate solutions.

The ability to predict the location of the shock from the oscillatory numerical solution and to reconstruct a monotonous solution in a postprocessing step allows one to develop globally higher-order-accurate numerical schemes for nonlinear hyperbolic equations, which in turn offers great potential in solving problems in gasdynamics, such as the Euler equations.

References

[1]Proot, M. M. J., "The Least-Squares Spectral Element Method—Theory, Implementation and Application to Incompressible Flows," Ph.D. Dissertation, Dept. of Aerospace Engineering, TU Delft, Delft, The Netherlands, Feb. 2003.

[2]Proot, M. M. J., and Gerritsma, M. I., "A Least-Squares Spectral Element Formulation for the Stokes Problem," *Journal of Scientific Computing*, Vol. 17, Nos. 1–4, 2002, pp. 285–296.

[3]Proot, M. M. J., and Gerritsma, M. I., "Least-Squares Spectral Elements Applied to the Stokes Problem," *Journal of Computational Physics*, Vol. 181, No. 2, 2002, pp. 454–477.

[4]Jiang, B. N., "A Least-Squares Finite Element Method for Incompressible Navier–Stokes Problems," *International Journal for Numerical Methods in Fluids*, Vol. 14, No. 7, 1992, pp. 843–859.

[5]Jiang, B. N., *The Least-Squares Finite Element Method, Theory and Applications in Computational Fluid Dynamics and Electromagnetics*, Springer-Verlag, Berlin, 1998.

[6]Jiang, B. N., "On the Least-Squares Method," *Computer Methods in Applied Mechanics and Engineering*, Vol. 152, Nos. 1–2, 1998, pp. 239–257.

[7]Jiang, B. N., and Chang, C. L., "Least-Squares Finite Elements for the Stokes Problem," *Computer Methods in Applied Mechanics and Engineering*, Vol. 78, No. 3, 1990, pp. 297–311.

[8]Jiang, B. N., Lin, T. L., and Povinelli, L. A., "Large-Scale Computation of Incompressible Viscous Flow by Least-Squares Finite Element Method," *Computer Methods in Applied Mechanics and Engineering*, Vol. 114, Nos. 3–4, 1994, pp. 213–231.

[9]Jiang, B. N., and Povinelli, L. A., "Least-Squares Finite Element Method for Fluid Dynamics," *Computer Methods in Applied Mechanics and Engineering*, Vol. 81, No. 1, 1990, pp. 13–37.

[10]Bochev, P., Cai, Z., Manteuffel, T. A., and McCormick, S. F., "Analysis of Velocity-Flux First Order System Least-Squares Principles for the Navier–Stokes Equations; Part I," *SIAM Journal on Numerical Analysis*, Vol. 35, No. 3, 1998, pp. 990–1009.

[11]Bochev, P., Manteuffel, T. A., and McCormick, S. F., "Analysis of Velocity-Flux First Order System Least-Squares Principles for the Navier–Stokes Equations: Part II," *SIAM Journal on Numerical Analysis*, Vol. 36, No. 4, 1999, pp. 1125–1144.

[12]Bochev, P. B., "Analysis of Least-Squares Finite Element Methods for the Navier–Stokes Equations," *SIAM Journal on Numerical Analysis*, Vol. 34, No. 5, 1997, pp. 1817–1844.

[13]Bochev, P. B., "Finite Element Methods Based on Least-Squares and Modified Variational Principles," Technical Rept. POSTECH, July 2001, http://com2mac.postech.ac.kr/Lecture/Lec-5.pdf.

[14]Bochev, P. B., and Gunzburger, M. D., "A Least-Squares Finite Element Method for the Navier–Stokes Equations," *Applied Mathematics Letters*, Vol. 6, No. 2, 1993, pp. 27–30.

[15]Bochev, P. B., and Gunzburger, M. D., "Analysis of Least-Squares Finite Element Methods for the Stokes Problem," *Mathematics of Computation*, Vol. 63, No. 208, 1994, pp. 479–506.

[16]Bochev, P. B., and Gunzburger, M. D., "Least-Squares Finite Element Methods for the Velocity-Pressure-Stress Formulation of the Stokes Equations," *Computer Methods in Applied Mechanics and Engineering*, Vol. 126, Nos. 3–4, 1995, pp. 267–287.

[17]Bochev, P. B., and Gunzburger, M. D., "Finite Element Methods of Least-Squares Type," *SIAM Review*, Vol. 40, No. 4, 1998, pp. 789–837.

[18]Canuto, C., Hussaini, M. Y., Quarteroni, A., and Zang, T. A., *Spectral Methods in Fluid Dynamics*, Springer Series in Computational Physics, Springer-Verlag, Berlin, 1987.

[19]Karniadakis, G. E., and Sherwin, S. J., *Spectral/hp Element Methods for CFD*, Oxford Univ. Press, Oxford, England, U.K., 1999.

[20]De Maerschalck, B., and Gerritsma, M. I., "The Use of the Chebyshev Approximation in the Space-Time Least-Squares Spectral Element Method," *Numerical Algorithms*, Vol. 38, No. 1, 2005, pp. 173–196.

[21]Laney, C. B., *Computational Gasdynamics*, Cambridge Univ. Press, Cambridge, England, U.K., 1998.

[22]Gottlieb, D., and Hesthaven, J. S., "Spectral Methods for Hyperbolic Problems," *Journal of Computational and Applied Mathematics*, Vol. 128, Nos. 1–2, 2001, pp. 83–131.

[23]Mason, J. C., and Handscomb, D. C., *Chebyshev Polynomials*, Chapman and Hall/CRC, Boca Raton, FL, 2003.

[24]Gottlieb, D., and Shu, C. W., "On the Gibbs Phenomenon and Its Resolution," *SIAM Review*, Vol. 39, No. 4, 1997, pp. 644–668.

[25]Gelb, A., and Tadmor, E., "Enhanced Spectral Viscosity Approximations for Conservation Laws," *Applied Numerical Mathematics*, Vol. 33, Nos. 1–4, 2000, pp. 3–21.

H. Atassi
Associate Editor